# JOURNAL OF ZANKOY SULAIMANI

Part -A- (Pure and Applied Sciences)

VOLUME 25 ISSUE 2 December 2023

ISSN: 1812-4100

www.jzs.univsul.edu.iq




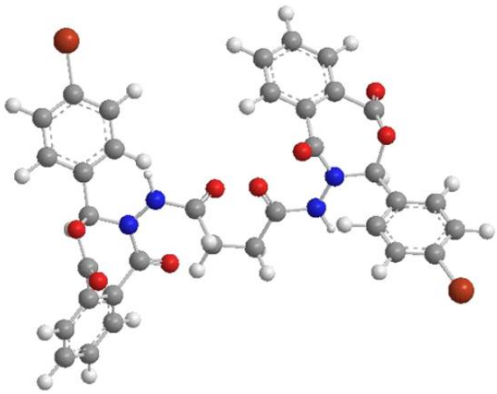

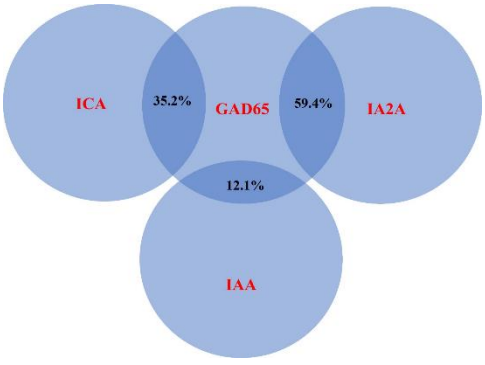


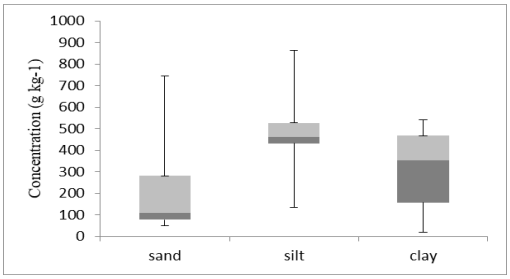

Journal homepage www.jzs.univsul.edu.iq
**Journal of Zankoy Sulaimani**
Part-A- (Pure and Applied Sciences)
ISSN:1812-4100

# Synthesis of Nanosized Zeolite Catalyst Particles from Waste Materials for Efficient Removal of Fe(III) from aqueous solution

Heman A. Smail*

*Department of Chemistry, College of Science, Salahaddin University, Erbil, Kurdistan Region, Iraq*
* Corresponding email: Heman.Smail@su.edu.krg

**Article info**

Original: 26/01/2023
Revised: 11/05/2023
Accepted: 20/05/2023
Published online: 20/12/2023

***Keywords:***
*ZSM-5 zeolite, nanocrystals, aluminum foil drug sachet waste, adsorption, iron*

**Abstract**

The objective of this study was to prepare zeolite ZSM-5 nanostructure from aluminum foil drug sachet waste by a simple conventional hydrothermal method using different times (24, 48, 72, and 96 h), and to figure out the adsorption capacity of zeolite ZSM-5 nanostructure for heavy metal of Fe(III) . The best time for synthesizing and testing the adsorption effectiveness of the provided ZSM-5 zeolite is 96 h. The ZSM-5 zeolite is defined by X-ray diffraction (XRD), Brunauer Emmett Teller (BET), Field Emission Scanning Electron Microscopy (FESEM) and Fourier transform infrared spectroscopy (FTIR) for confirming their structure and properties, such as crystal structure, surface area, and surface morphology. The crystallinity percentage of nanosized ZSM-5 was 100%, and the surface area and micropore volume were 368.70 $m^2/g$ and 0.158 $cm^3/g$, respectively. In addition, the ZSM-5's adsorption efficiency the solution for Fe(III) was tested. Many factors, including adsorption properties, contact duration, initial iron solution content, and pH, were investigated. The equilibrium was reached after 25 minutes. pH levels between 3.0 and 4.0 were shown to be optimal for the absorption of iron solution. The iron species` adsorption capacities in solutions at 298 K were 56.49 mg/g, at 308 K, 86.20 mg/g, and at 318 K, 68.02 mg/g. The findings of the Freundlich adsorptions and Langmuir were used to represent the isotherm constants. The Langmuir model can adequately describe the Fe(III) solutions` adsorption isotherm data while testing at 298K and 308K, whereas those of Fe(III) testing at 308K and 318K were more closely connected to the Freundlich model.

## Introduction

Zeolites, an aluminosilicate mineral that is microporous and crystalline, are also referred to as "molecular sieves." Zeolite features three-dimensional structures made of networks of $[SiO_4]^{4-}$ and $[AlO_4]^{5-}$ tetrahedral atoms that are connected to one another by oxygen atoms (1). For applications in catalysis, zeolite nanoparticles (NP, 10-100 nm) are viable substitutes for traditional micrometric zeolite particles because their greater exterior surface area ensures better dispersion of reactants and products (2). ZSM-5 zeolites, which are nanosized and have a large surface area and a well-characterized microporous structure, are widely used in many sectors. Because of its superior thermal stability and distinctive pore structure, ZSM-5 zeolite, one of the most significant materials of crystalline microporous, has found extensive usage in the disciplines of coal chemistry, petrochemistry, adsorption, and ion exchange (3). The zeolites were defined by their size, shape, and channeling, as well as their well-characterized structures of porosity. Their porosity, which was less than 2.0 nm, was categorized as microporous materials (4). Numerous uses, including an adsorbent in wastewater involving catalyst support, ion-exchange: capability, and inorganic and organic contaminants, benefit from these dominating features (5, 6). Because of their simplicity of product separation, high-

pressure resistance, thermal stability, and mechanical strength, when it comes to practical uses, zeolites are among the most popular in the numerous industrial chemical processes including petroleum cracking, isomerization, and alkylation reactions (7). When used as catalysts, zeolites are typically mixed with transition metals with abundant electrons in the d orbital, including iron (Fe), copper (Cu), and platinum (Pt). These metals, including Fe/NaY, Fe/MOR, Fe/MCM-48, Fe/MCM-41, and Fe/ZSM-5, operating as promoters and converted into cationic form to improve the performance of the active and/or support sites (8, 9). The phenol hydroxylation process, which results in the production of two benzenediols ($C_6H_4(OH)_2$) based on the reaction of hydrogen peroxide ($H_2O_2$) and phenol ($C_6H_5OH$), and comprising hydroquinone and catechol, has been studied on these catalysts. These goods may be used for a variety of purposes, such as polymerization inhibitors, antioxidants, and photography chemicals (10). According to the level of (Fe) loading, pore size, and zeolite surface area, the selectivity of the products and the rate of phenol conversion compared with the reaction time varied. But with time, the catalysts somewhat lost their effectiveness, most probably as a result of the covering of carbon on the zeolites surface and/or the development of coke from the blockage (11). On the other hand, high-temperature processing might have an impact on metal sintering, leading to remove a metal dispersion and greater metal size (12). The catalyst has to be manufactured in line with the unique characteristics of every zeolite in order to reduce these problems. The method used to prepare the catalyst has an impact on its qualities. The physical characteristics of each zeolite, including its durability, stability, and surface area, must then be considered throughout the preparation stage. A great contact between the zeolite and the metal is produced by an effective preparation technique, which leads to increased activities in the active sites, less catalyst sintering, and improved metal dispersion (6). The ion-exchange or adsorption caused by the zeolites being negatively charged, greater than the level of their zero charge (PZC), if they are disseminated in solution is one of the most popular techniques for creating supported zeolites on catalysts. The outcome allowed for the metal to engage with it in cation form and dissolve within a solution (12). Nearly all forms of water include iron Fe(III), such as drinking and surface water, although other kinds of water, including water-tube boilers and water utilized in systems of heating, do not. In addition, iron is considered as a biogenic component. Because of precipitation in systems of water distribution, its elimination has been extensively explored (13). Fe(III), which makes up 95% (w/w) of the world's metal output, is one of the most widely utilized metals due to its cheap cost and toughness. An unpleasant odor, an unpleasant taste, and turbidity are all effects of too much Fe(III) in water, particularly in public water sources. It stains fixtures of plumbing and gives cleaned clothes and materials a brownish tint. Additionally, it complicates systems of distribution by fostering the development of iron bacteria, which clogs pipes and raises the coefficient of rugosity (14). As a consequence, the use of Fe(III) is restricted in some sectors, including industries of remove the, textile, and food. Despite being present in high proportions in an insoluble form in nature, iron may be transformed into soluble forms, which often contaminate water (15). In addition to iron removal, the best zeolites are also often employed to remove other inorganic contaminants and heavy metals. With a high absorption of Fe(III), zeolites are adsorbents because of their stability, affinity to metal cations, and great capacity for ion exchange under varied conditions of chemical and physical (16). There are different ways to prepare such zeolites compounds using the hydrothermal method (17-20). But these methods depend on the use of high-cost chemicals for aluminum sources. So this was motivating me to work at that point. In this research paper. Thus, the novelty in this work, aluminum foil drug sachet waste was used to nanosynthesize ZSM-5 zeolite 100% with a high surface area. Later, the properties of phase surface and structure in the ZSM-5 zeolite were evaluated through FTIR, nitrogen adsorption-desorption, FESEM, and X-ray diffraction (XRD). The ZSM-5 zeolite's ability to absorb Fe(III) from the solution also was examined. We examined the pH, adsorption time, and influences of temperature, which were distinct.

## Materials and methods

### *Chemicals*

Aluminum foil drug sachet waste was utilized as an alumina source. To aid in the zeolite framework formation as template reagents, NaOH (Sigma-Aldrich), Silicon dioxide, 99%, Honeywell Fluka™ ($FeCl_3$ $6H_2O$, Merck), Tetrapropyl Ammonium Bromide (TPABr, Merck), and Tetrpropylammonium Hydroxide (TPAOH, 20% Fluka) were utilized.

### *Synthesis of zeolite nanostructures*

A Slight modification was made in the hydrothermal synthesis of ZSM-5 nano-zeolite from the previously reported literature (21). ZSM-5 nanozeolite was synthesized utilizing silicon dioxide and aluminum foil drug sachet waste. To aid in the zeolite framework formation as template reagents, tetrapropylammonium bromide (TPABr) and Tetrapropylammonium hydroxide (TPAOH)were utilized. Usually, 70.0 g of water is used to dissolve 4.2 g of sodium hydroxide, which is then split into two equal pieces. To thoroughly dissolve 25 g of silicon dioxide, one part of sodium hydroxide solution was employed, and the resulting suspension was therefore agitated for obtaining a clear solution. The solution of sodium silicate was then given 18.0 g of 20% tetrapropylammonium hydroxide where being stirred. After that, for an additional hour, the mixture has been stirred. 2.0 g of aluminum foil drug sachet trash was combined with some more NaOH solution to create an aluminate solution. The solution of silicate was progressively added into the solution of aluminate whilst being violently agitated when the solutions had acquired the appropriate clarity. The resulting mixture was agitated for 1 hour before being put into stainless steel autoclaves coated with Teflon and subjected to hydrothermal synthesis at 150 °C for 24, 48, 72, and 96 hours. The products of solid were then filtered, repeatedly rinsed using distilled water till the pH value fell to 8.2, and dried overnight at 120 °C in an oven.

### *Adsorption studies*

Applying 0.015 g of zeolite ZSM-5, for the impact of initial ferric ion concentration and adsorption tests of contact time were conducted with a system of the 25mL solution involving variations in the concentration of $FeCl_3.6H_2O$ within 70 minutes of contact time that were 5, 10, 15, 25, 35, 45, 55 and 20, 40, 60 and 80 mg/L. For adjusting the pH to 2.00, 2.50, 3.00, 3.50, 4.00, 5.00, and 6.00, in every flask, a solution of 0.10 M NaOH and a solution of 0.10M HCI were mixed then added to the solution of ferric ion. A water bath was used to heat the mixture with a constant temperature vibrator set at a specific temperature (298K, 308K, and 318K) for 60 minutes. The pH of the solutions was set to 3.50, and for the adsorption isotherm, the concentrations of Fe(III) were changed from 10.00 to 75.00mg/L. To remove the adsorbent from the solutions, they were filtered. At a wavelength of 248.3 nm, before and after contacting zeolite ZSM-5, the concentration of metal ion was determined, utilizing a spectrometer of atomic absorption (GBC 932 Plus). Equation (1) was used to compute the values in order to get the total capacity of adsorption of Fe (III) measured at equilibrium (22).

$$q_e = \left(\frac{C_o - C_e}{w}\right) * V \qquad (1)$$

Where $C_o$ (mg/L) is the initial Fe(III) concentration, $C_e$ (mg/L) is the equilibrium Fe(III) concentration, W (g) is the weight of ZSM-5 zeolite, $q_e$ (mg/g) represents the equilibrium adsorption capacity of ferric ion adsorbed on the mass of ZSM-5 zeo1ite, and V (L) represents the Fe(III) solution volume.

### *Characterization of ZSM-5*

At 20 °C, XRD patterns of as-prepared samples of zeolite nanostructures (ZSM-5) were detected using CuKα radiation= 0.154 nm at a current of 35 mA and 45 kV (D5000 by the diffraction of X-rays, Germany). The FTIR spectra of the zeolite nanostructures as-prepared samples were gathered through a KBr disk and a (USA, MA, Waltham, PerkinElmer model Spectrum One) spectrophotometer. A scanning electron microscope (ZEISS SIGMA-Belgium) was used to capture FESEM images of the zeolite nanostructures as-

prepared samples. Utilizing BET method, identified surface of the nanozeolite was measured on the Engage Micromeritics (3FLEX, GA, USA) Nitrogen Adsorption Instrument.

## Results and discussion

### *ZSM-5 nanozeolite Characterization*

The peaks in (Figure 1). Illustrate the pattern of XRD powder image ZSM-5 nanozeolite. The major peaks` analysis at 2θ = 7.85°, 8.80°, 15.85, 23.05°, 24.40° and 29.85 based on the standard data from JCPDS 44-0003 revealed the obtaining of pure ZSM-5 nanozeolite. As illustrated in (Table 1). The nanometer size of the zeolite crystals size (D, nm) of the nanoparticles using the Scherrer equation and the percentage of crystallinity is given by the relationship in equations (2 and 3), respectively:

$$D = \frac{k*\lambda}{\beta \cos(\theta_\circ/2)} \quad (2)$$

$$Crystallinity\ \% = \frac{\sum Intensity\ of\ peaks\ of\ zeolite}{\sum Intensity\ of\ peaks\ of\ Standard} * 100 \quad (3)$$

in which λ is the wave-length of the incident x-rays, β, the full width at half maximum (FWHM) of the diffraction peak and $\theta_\circ$, the angle between the diffracted and the incident ray.$k$ is a constant whose value Scherrer's (0.9 ) revealed that this product is composed of spherical shaped aggregates (23).

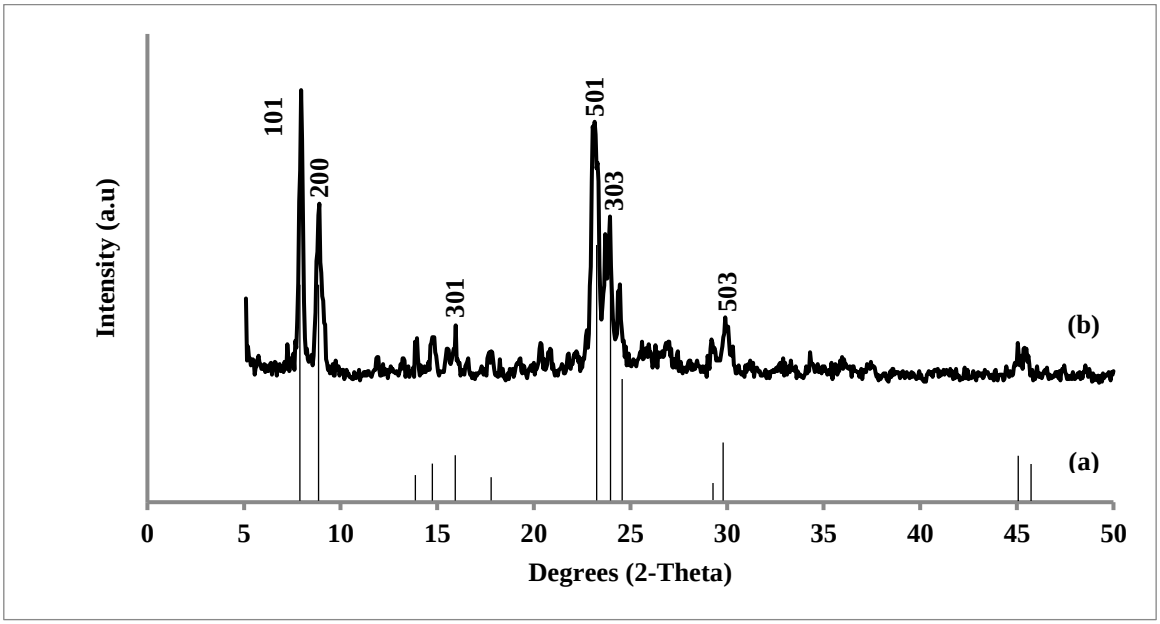


**Figure 1**: XRD pattern of the ZSM-5 nanoparticle (a) Standard, (b) Synthesized

### *Study of FTIR*

Figure 2 illustrated the FTIR spectra of a synthesized ZSM-5 nanozeolite. Around 460 $cm^{-1}$, 550 $cm^{-1}$, 799 $cm^{-1}$, 1013 $cm^{-1}$, and 1239 $cm^{-1}$ are the typical skeletal vibration peaks of ZSM-5 zeolite. The ZSM-5 FTIR spectrogram is comparable with those that were reported by (24). Additionally, water in the zeolite causes a stretching vibration peak of water molecules around 1647 $cm^{-1}$ and an OH vibration peak at 3486 $cm^{-1}$.

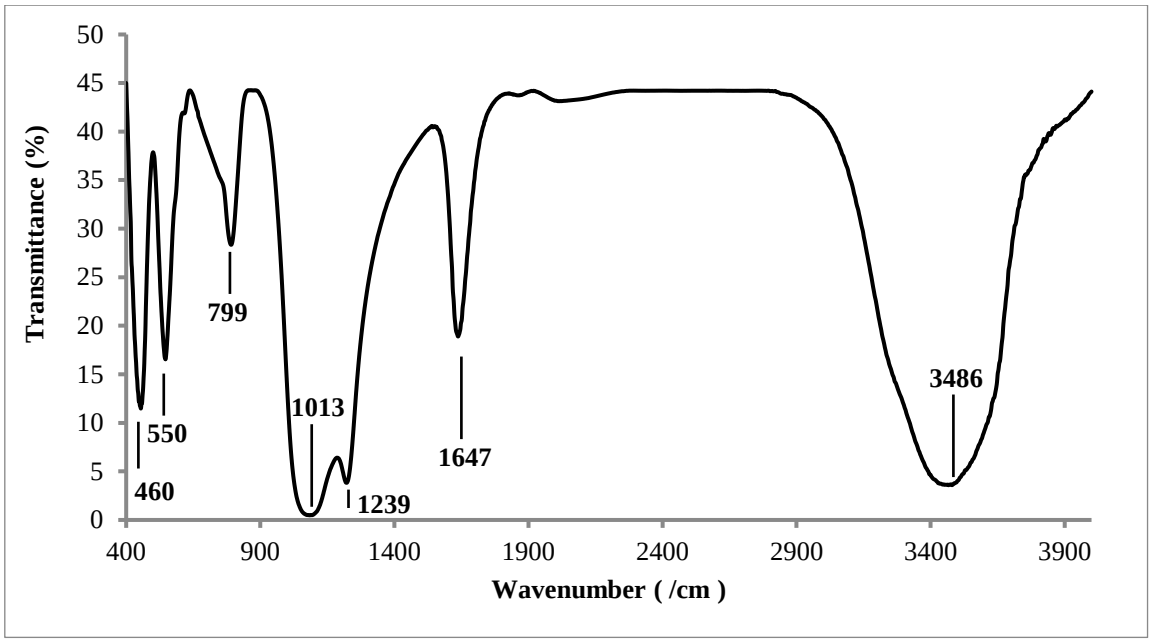


**Figure 2**: FTIR spectrum of ZSM-5 nanoparticle

*The surface area (BET) analysis*

$N_2$ desorption and adsorption were employed to estimate the ZSM-5 crystals` pore volume and surface area. The prepared ZSM-5's isotherm and pore size distribution curve was illustrated in (Figures 3 (a) and (b) ). Because of the filling of micropores, the $N_2$ adsorption/desorption isotherm of ZSM-5 zeo1ite exhibits a pronounced knee at p/p° less than 0.1. The factors from the t-plot approach and BET equation, such as total volume of pore, volume of micropore, percentages of microporosity, micropores size, the BET surface area, and are illustrated in (Table 1). The curve fit an isotherm of type V with a steep step and showed a B-type loop at relative pressures of p/p° = 0.4-0.5. It implied that the product was heaped onto a crystal and that the stacking process created an opening secondary pore structure. ZSM-5 has a surface area of 368.70 $m^2/g$ and a micropore volume of 0.158 $cm^3/g$. As illustrated in (Figure 3b). According to the curve, the mean size of the zeolite's micropores was calculated to be roughly 0.5 nm. The isotherm curve of $N_2$ adsorption showed a clear hysteresis loop, which was comparable to the outcome previously described (25, 26).

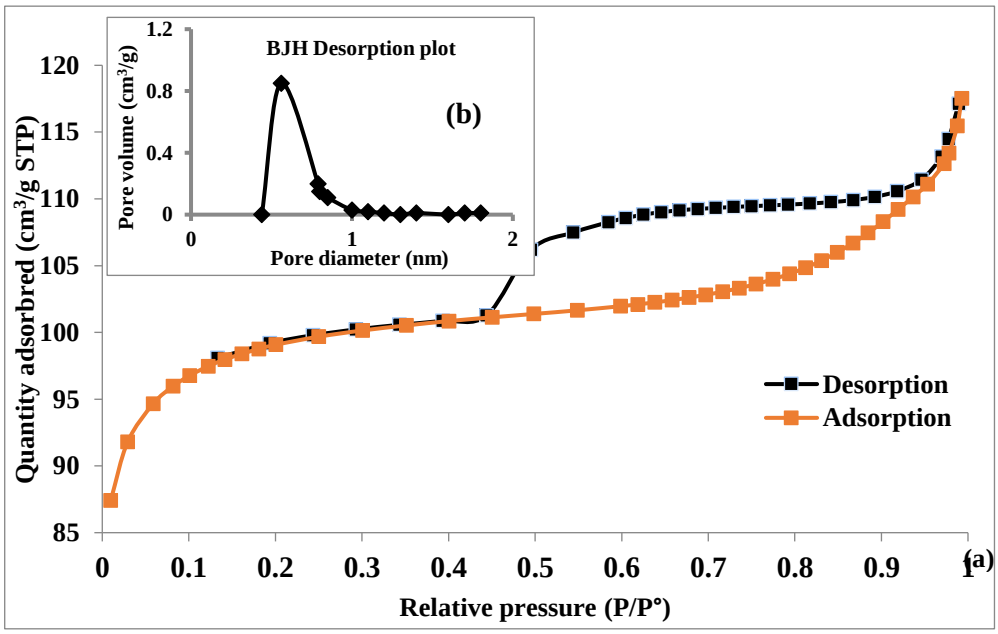


**Figure 3:** (a) $N_2$ adsorption-Desorption isotherm a, (b) pore size distribution curve of synthesized ZSM-5 nanoparticle.

**Table 1**: Surface texturing, crystallite size, and crystallinity % data of ZSM-5 zeolites provided from aluminum foil drug sachet waste.

| Sample | BET surface[a] area ($m^2/g$) | Total pore volume ($m^3/g$) at $p/p_o$= (0.05–0.3) | Micropore volume[b] ($m^3/g$) | Microporosity[d] (%) | Size of Micropores[c] (nm) | crystallite size(D,nm) | Crystallinity (%) |
|---|---|---|---|---|---|---|---|
| ZSM-5 nanosized | 368.70 | 0.163 | 0.158 | 96.93 | 0.52 | 24.46 | 100.00 |

[a] BET method.

[b and c] Micropore volume and Size of micropores determined by t-Plot method.

[d] Microporosity percentages = (Micropore volume / Total porevolume) * 100.

## *Study of Field Emission Scanning Electron Microscopy*

Figure 4 is morphologies of the produced ZSM-5 zeolite demonstrate that it crystallizes into crystals of spherical-shaped *(27)*. The spherical-shaped diameter that we successfully obtained, ZSM-5 nanoparticles, was, according to the FESEM image, 34.75 nm in size. Nevertheless, utilizing the Scherer equation and X-ray data, the crystal's predicted crystalline size is 24.46 nm. Although a particle may be polycrystalline, the Scherer equation's calculation of crystalline size pertains to a single ZSM-5 framework crystal size. When each particle is a single crystal, then the crystal size is the same as the particle size. The particles of polycrystalline zeolite used in this work have crystal sizes that are submultiples of the particle size (28).

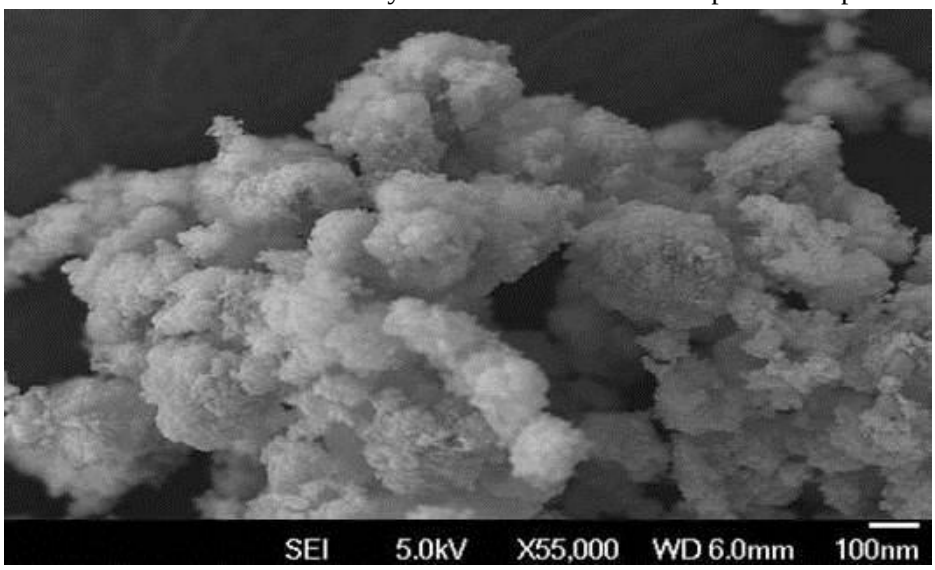


**Figure 4**: FESEM image of ZSM-5 nanoparticle zeolite

## *Fe(III) adsorption study*

Impact of concentration of Fe(III) and contact time.

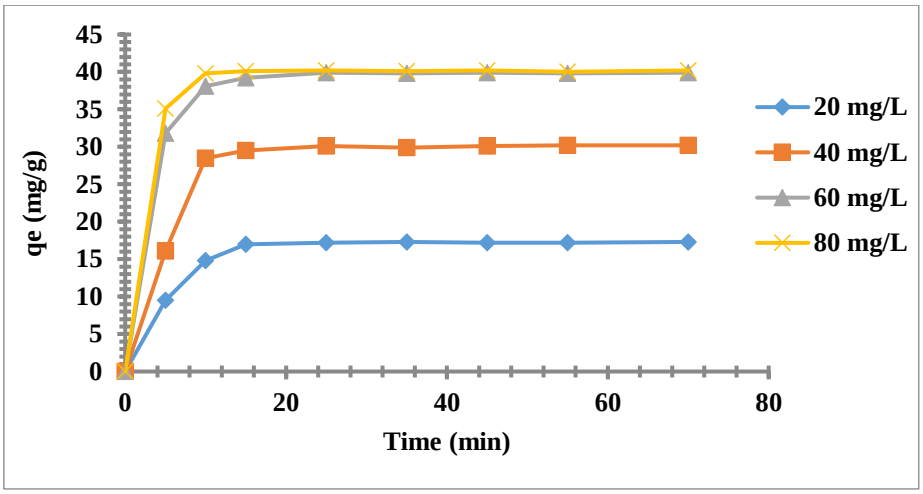


**Figure 5**: Time-dependent adsorption capacity for varying initial concentrations.

Figure 5 depicts the remove of ferric ion adsorption capacity as a contact time minute function at various initial concentrations. At first, the Fe(III) was rapidly adsorbed onto the adsorbent surface because adsorption sites were available. However, as the adsorption sites were filled, the Fe(III) adsorption rate stabilized and reached equilibrium after 25 minutes (29). Based on the rise in mass transfer or propulsion, when the concentrations of the Fe(Ill) grew, the capacity of adsorption of the Fe(III) rose as follows: 17.20, 30.10, 39.90, and 40.20 mg/g. However, because the concentrations came to saturation, the adsorption capacity of ferric ion somewhat increased as the concentration increased from 60.00mg/L to 80mg/L. Therefore, the primary Fe(III) solution concentration was set at 60.00 mg/L for following evaluation of the influence that adsorbent level and pH had on the adsorption of Fe(III) (30).

## The pH-dependent impact on the Fe (III) adsorption

The influence of pH on Fe(III) adsorption is displayed in (Figure 6). With the optimal value being between 3.0 and 4.0, when the ferric ion solution pH rose from 2.0 to 3.5. When the pH was raised from 4.0 to 6.0, the Fe(III) solution adsorption effectiveness dropped. Competitive adsorption between Fe(III) and $H^+$ on ZSM-5 zeolite surface may be to blame for the reduced capacity of adsorption at pH 2.0 and 2.5. The main reason for the reduced capacity of adsorption at pH 5.0 and 6.0 was the conversion of ferric ion to predominantly ferric hydroxide species, which is seldom soluble in water. The tiny level of adsorption seen with the rise in pH value from 5.0 to 6.0 was quite likely owing to the existence of additional $Fe(OH)_2^+$, $Fe(OH)_4^-$ and ion species, and that is compatible with literature study by (31).

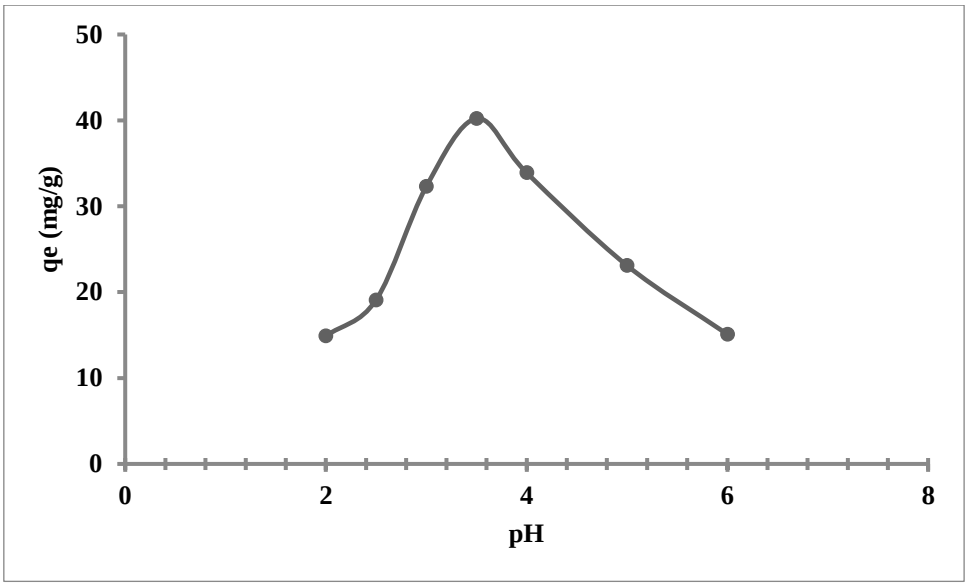


**Figure 6**: Effect of pH on adsorption capacity

## Adsorption isotherm

In this experiment, the impact of temperature on the isotherm of adsorption was studied from 298K to 318 K. The obtained data were analyzed to determine the relationship between the equilibrium Fe(III) concentration and unit mass equilibrium adsorption capacity of Fe(III) on ZSM-5 zeolite utilizing two adsorption isotherms chosen from the isotherm models of Freundlich and Langmuir, as illustrated in equations (4) and (5). The Langmuir equation`s linear version underlies the isotherm of Langmuir, which assumes that adsorption happens inside the adsorbent at discrete homogenous sites (32).

$$\frac{Ce}{qe} = \frac{1}{KL\ qm} + \frac{1}{qm} * Ce \qquad (4)$$

$$\ln qe = \ln K_F \ + \frac{1}{n} * \ln Ce \quad (5)$$

In this equation, $K_F$ (L/g) represents the equilibrium constant of Freundlich isotherm, $q_e$ (mg/g) represents capacity of equilibrium adsorption of the ferric ion adsorbed on the unit mass of the ZSM-5 zeo1ite, $q_m$ (mg/g) represents capacity of maximum adsorption, $C_e$ (mg/L) represents equilibrium concentrations of the ferric ion, and $K_L$ (L/mg) is the equilibrium constant of Langmuir (33). (Figures 7 and 8). Depict the Fe(III) adsorption isotherms tested at 298K, 308K, and 318K respectively. The data were fitted using the models of Langmuir and Freundlich isotherm. Based on the findings, the correlation coefficients ($R^2$) at 298K and 308K for the Fe(III) solution adsorption isotherms were near to one when fitted by the Langmuir isotherm. However, as shown in (Table 2). The adsorption of ferric ion at 308 and 318 K, was well represented by the Freundlich model. As a result of the evidence, both chemisorption and physisorption might have a function in the occurrence of an adsorption phenomena. Calculating the factor of separation, also known as the equilibrium parameter ($R_L$), a dimensionless constant, allows one to determine the fundamental property of the Langmuir isotherm:

$$R_L = \frac{1}{1 + K_L\ C_o} \qquad (6)$$

where ($C_o$ and $K_L$) are as defined in equations (1) and (4). The following outcomes are possible for $R_L$'s value *(34)*.defined $R_L$ = 1 as linear adsorption, $R_L$ = 0 as irreversible adsorption, $0<R_L<1$ as favorable adsorption,

and $R_L$>1 as unfavorable adsorption. As illustrated in (Table 2). Equation (6) was used to compute the values of $R_L$ (Table 2). Shows that the values of $R_L$ range from 0 to 1, which are indicative of an adsorption of favorable. The value of n in the Freundlich model is higher than one (n > 1). This might be due to sites distribution of surface or any other reason that reduces interaction of adsorbent-adsorbate when surface density increases (35). The first adsorption was monolayer chemisorption, and it happened quickly on a silanol group (-OH) that was present in ZSM-5 in abundance. The silanol functional group (-OH) in ZSM-5 was lowered, leading to a lesser electrostatic interaction, which reduced the rate of adsorption. Later, physisorption, a weaker kind of adsorption, became prevalent and was probably released by the increased temperature and energy (36, 37).

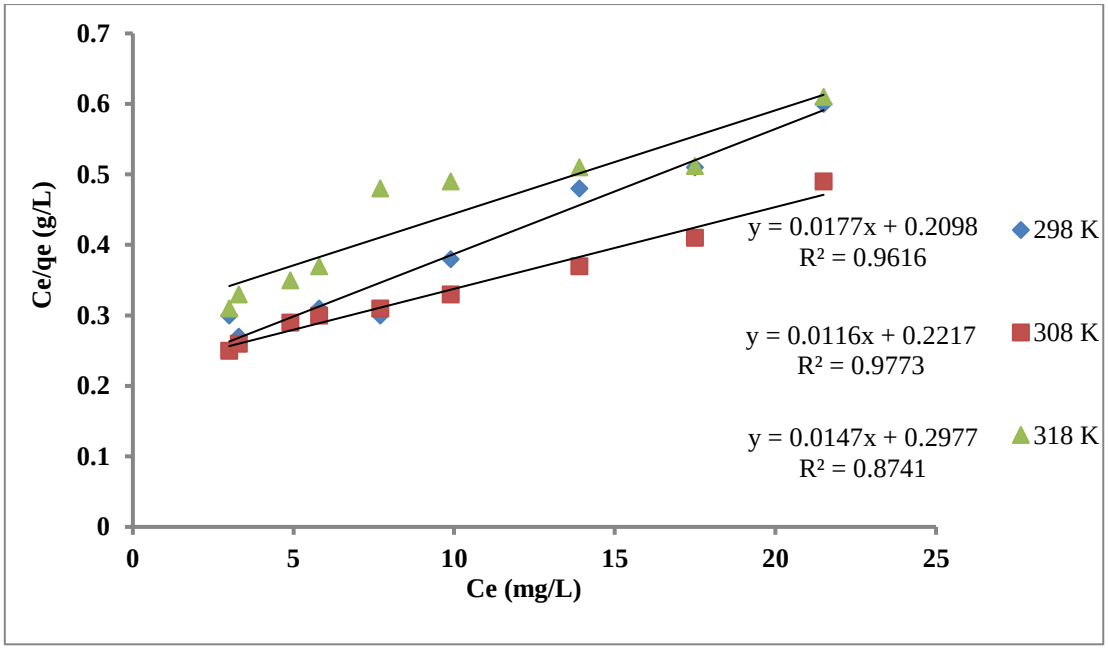


**Figure 7**: Langmuir adsorption Isotherm of Fe(III) by ZSM-5 nanoparticle zeolite

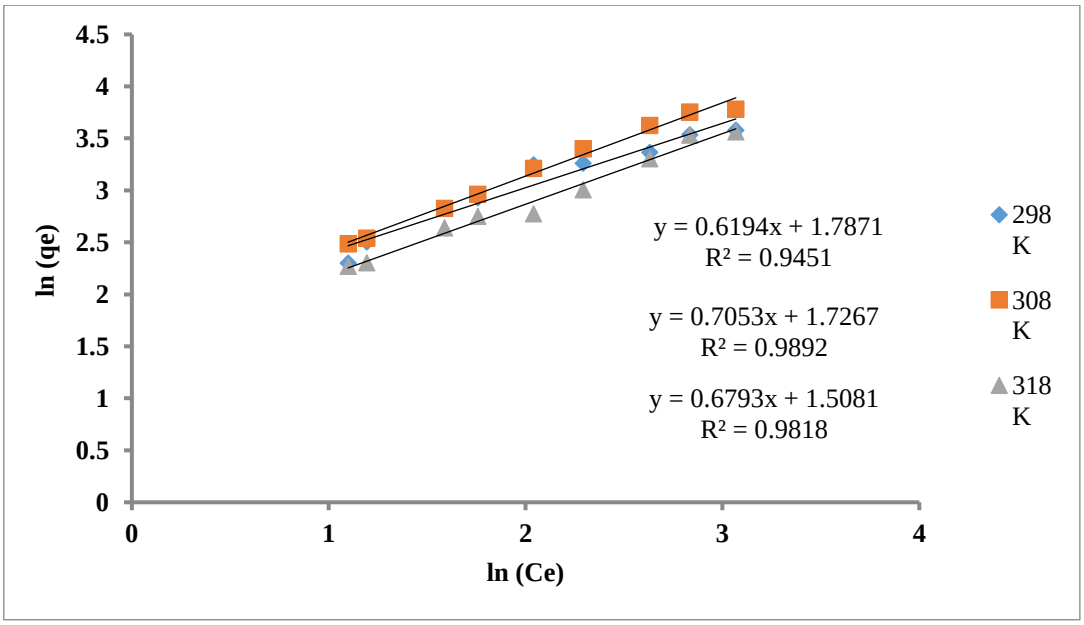


**Figure 8**: Freundlich adsorption Isotherm of Fe(III) by ZSM-5 nanoparticle zeolite

**Table 2**: Parameters of adsorption isotherm of Fe (III) on ZSM-5 nanozeolite

| Temperature(K) | Langmuir isotherm | | | | Freundlich isotherm | | |
|---|---|---|---|---|---|---|---|
| | $q_m$ (mg/g ) | $K_L$ (L/mg) | $R^2$ | $R_L$ | $K_F$ (L/g) | n | $R^2$ |
| 298 | 56.4971 | 0.0843 | 0.9616 | 0.1650 | 0.5805 | 1.6144 | 0.9451 |
| 308 | 86.2068 | 0.0523 | 0.9773 | 0.2416 | 0.5462 | 1.4178 | 0.9892 |
| 318 | 68.0272 | 0.0493 | 0.8741 | 0.2526 | 0.4108 | 1.4721 | 0.9818 |

## Conclusions

Hydrothermal synthesis of the pure ZSM-5 zeolite nanostructure is accomplished effectively utilizing aluminum foil drug sachet waste as raw material. It was discovered that 96 h is the best time for synthesizing ZSM-5 zeolite. Investigations were done on the ZSM-5 zeolite's capacity to adsorb Fe(III) from aqueous solutions. The zeolite of ZSM-5 can be utilized as an adsorbent for adsorption of Fe(III) in various optimized situations, such as temperature, the Fe(III) solution pH, initial concentration, and contact time. After 25 minutes of interaction, equilibrium was reached. For Fe(III) adsorption, the optimum pH was between 3.0 and 4.0, because the competitive adsorption between hydrogen ion and ferric ion was less intense at lower pH levels and the precipitation of ferric ion was stronger at higher pH levels as shown in Table 2. Shows increasing adsorption capacity when raising temperature from 298 K to 308 K, but then it decreased at 318 K. The Fe(III) adsorption isotherms tested at 298K and 308K were a good match with the model of Langmuir, but the adsorption isotherms of the Fe(III) assessed at 308K and 318K were possibly related to the Fruendlich model, implying the presence of both physical and chemical adsorption processes. In the future works would be required to optimize the best condition to synthesise new catalyst in the field of medicine, pharmacology, petroleum industries and environmental remediation.

## Conflict of interest

The authors confirm that they are not affiliated with or involved in any organization or entity with financial interests.

## Acknowledgements

The author acknowledges the Ibnu Sina Institute for Fundamental Science Studies at the University of Technology in Malaysia.

## References

1. Abdul K, Alam MM, Hoque M, Mondal S, Bin HJ, Xu B, Johir MAH, Karmakar AK, Zhou JL, Ahmed MB, Moni AM. (2020). Zeolite synthesis from low-cost materials and environmental applications: A review. Environmental Advances, 2:100019.

2. Moussa BO, Borghol I, Hu D, Casale S, Millot Y, Sayag C, Blanchard J, Olivier D. (2019). Synthesis of supported ZSM-5 nanoparticles. Microporous and Mesoporous Materials, 287:177-182.

3. Chen X, Jiang R, Gao Y, Zhou Z, Wang X. (2021). Synthesis of nano-ZSM-5 zeolite via a dry gel conversion crystallization process and its application in MTO reaction. Crystal engineering communication; 23, 2793-2800.

4. Zhang C, Fan K, Ma G, Lei C, Xu W, Jiang J, Sun B, Zhang H, Zhu Y, Song WS. (2021). Efficient Synthesis of Mesoporous Nano ZSM-5 Zeolite Crystals without a Mesoscale Template. Crystals; 11(10): 2-10.

5. Osako N, Pansakdanon C, Sosa N, Dekamwong K, Keawkumae C, Ronchapo W, Chanlek N, Jusamath J, Prayoonpukarach S, Wittayakun J. (2017). Characterization and comprehension of zeolite NaY/mesoporous SBA-15 composite as adsorbent for paraquat. Materials Chemistry and Physics; 193: 470-476.
6. Rakmae S, Keawkumay C, Osakoo N, Montalbo K, Leon R. L, Kidkhunthod P, Chanlek N, Roessner F, Prayoonpokarach S, Wittayakun J. (2016). Realization of active species in potassium catalysts on zeolite NaY prepared by ultrasound-assisted impregnation with acetate buffer and improved performance in transesterification of palm oil. Fuel; 184:512-517.
7. Wang Y, Kikhtyanin O, Li C, Su X, Bai X, Wu W. (2021). Synthesis of Nanosized ZSM-5 Zeolites by Different Methods and Their Catalytic Performance in the Alkylation of Naphthalene. Advanced Molecular Sieves; 3(1): 149-160.
8. Villa AL, César AC, Montes C. (2005). Cu- & Fe-ZSM-5 as catalysts for phenol hydroxylation. Journal of Molecular Catalysis A: Chemical; 228(1-2): 233-240.
9. Zhao W, Yunfei L, Peng D, Quanzhi L. (2001). Synthesis of Fe-MCM-48 & its catalytic performance in phenol hydroxylation. Catalysis Letters; 73(2): 199-202.
10. Brook M, Andrew C, Laurence S, John R, Lindsay H, Raymond M, Kenneth P. (1982). Aromatic hydroxylation. Part 7. Oxidation of some benzenoid compounds by iron compounds and hydrogen peroxide with the aromatic compound acting as substrate and solvent. Journal of the Chemical Society Perkin Transactions; 2: 687-692.
11. Kosri C, Deekamwong K, Sophiphun O, Osakoo N, Chanlek N, Föttinger K, Wittayakun J. (2017). Comparison of Fe/HBEA catalysts from incipient wetness impregnation with various loading on phenol hydroxylation. Reaction Kinetics, Mechanisms and Catalysis; 121(2): 751-761.
12. Mäki-Arvela P, Murzin DY. (2013). Effect of catalyst synthesis conditions on the metal particle size. Applied Catalysis.A: General; 451: 251-281.
13. Qiu W, Li W, He J, Zhao H, Liu X, Yuan Y. (2018). Variations regularity of microorganisms and corrosion of cast iron in water distribution system. Journal of Environmental Sciences China; 74: 177-185.
14. Onganer Y, Temur Ç. Adsorption dynamics of Fe(III) from aqueous solutions onto activated carbon. Journal of Colloid and Interface Science 1998; 205(2): 241-244.
15. Indianara C, Ostroski M, Barros ASD, Edson A, Silva JH, Dantas PA, Arroyo O, Lima CM. (2009). A comparative study for the ion exchange of Fe(III) and Zn(II) on zeolite NaY. Journal of Hazardous Materials; 161(2-3): 1404-1412.
16. Tomáš B, Mária K, Anna G, Henrieta P, Rudolf H, Zuzana H. (2020). Characterization of Fe (III) Adsorption onto Zeolite and Bentonite. International Journal of Environmental Research and Public Health; 17:(16). 1-13.
17. Mu Y, Zhang Y, Fan J, Guo C. (2017). Effect of ultrasound pretreatment on the hydrothermal synthesis of SSZ-13 zeolite. Ultrasonics Sonochemistry; 38: 430-436.
18. Anbia M, Koohsaryan E, Borhani A. (2017). Novel hydrothermal synthesis of hierarchically structured zeolite LTA microspheres. Materials Chemistry and Physics; 193: 380-390.
19. Sousa LV, Silva AOS, Silva BJB, Teixeira CM, Arcanjo APR, Pacheco JGA. (2017). Fast synthesis of ZSM-22 zeolite by the seed-assisted method of crystallization with methanol. Microporous and Mesoporous Materials; 254: 192-200.
20. Bortolatto LB, Boca Santa RAA, Moreira JC, Machado DB, Martins MAPM, Fiori MA, Kuhnen NC, Riella HG. (2017). Synthesis and characterization of Y zeolites from alternative silicon and aluminium sources. Microporous and Mesoporous Materials; 248: 214-221.
21. Fan W, Morozumi K, Kimura R, Yokoi T, Okubo T. (2008). Synthesis of nanometer-sized sodalite without adding organic additives. Langmuir; 24(13): 6952-6958.
22. Wang J, Chen C. (2006). Biosorption of heavy metals by Saccharomyces cerevisiae: a review. Biotechnology advances; 24(5): 427-51.
23. Nassar MY, Aly HM, Abdelrahman EA, Moustafa ME. (2017). Synthesis, characterization, and biological activity of some novel Schiff bases and their Co(II) and Ni(II) complexes: A new route for $Co_3O_4$

and NiO nanoparticles for photocatalytic degradation of methylene blue dye. Journal of Molecular Structure; 1143: 462-471.
24. Pan F, Lu X, WangY, Chen S, Wang T, Yan Y. (2014). Organic template-free synthesis of ZSM-5 zeolite from coal-series kaolinite. Materials letters; 115: 5-8.
25. Chen H, Xiangwen Z, Junfeng Z, Qingfa W. (2017). Controllable synthesis of hierarchical ZSM-5 for hydroconversion of vegetable oil to aviation fuel-like hydrocarbons. Royal Society of Chemistry Advances; 7: 46109-46117.
26. Wang XG, Shao DD, Hou GS, Wang X K, Ahmed A, Ahmad B. (2015). Uptake of Pb(II) andU(VI) ions from aqueous solutions by the ZSM-5 zeolite. Journal of Molecular Liquids; 207: 338-342.
27. Mohamed RM, Fouad OA, Ismail AA, Ibrahim IA. (2005b). Influence of crystallization times on the synthesis of nanosized ZSM-5. Materials letters; 59(27): 3441-3444.
28. Wang D, Li X, Liu Z, Zhang Y, Xie Z, Tang Y. (2010). Hierarchical structured ZSM-5 zeolite of oriented nanorods and its performance in the alkylation of phenol with isopropanol. Journal of colloid and interface science; 350(1): 290-294.
29. Wang L, Zhang J, Zhao R, Li Y, Zhang C. (2010). Adsorption of Fe on activated carbon prepared from polygonumorientale Linn.: Kinatic, Isotherm, pH,and ionic strength studies. Bioresource Technology; 101(15): 5808-5814.
30. Hashemian S, Hossiene SH, Salehifar H, Salar I K. (2013). Adsorption of Fe(III) from Aqueous Solution by Linde Type-A Zeolite. American Journal of Analytical Chemistry; 4(7A): 123-126.
31. Deng R, Hu Y, Zuo W, Ku J. (2017). Adsorption of Fe(III) on smithsonite surfaces and implications for flotation. Colloids and Surfaces A Physicochemical and Engineering Aspects; 533: 308-315.
32. Zhang X, Bai R. (2003). Mechanism & kinetics of humic acid adsorption onto chitosan coated granules. Journal of Colloid and Interface Science; 264(1): 30-38.
33. Frimmel FH, Huber L. (1996). Influence of humic substances on the aquatic adsorption of heavy metals on defined mineral phases. Environmental International; 22(5): 507-517.
34. Senturk HB, Ozdes D, Duran C. (2010). Biosorption of rhodamine 6G from aqueous solutions onto almond shell. Desalination; 252(1-3): 81-87.
35. Reed B, Matsumoto M. (1993). Modeling cadmium adsorption by activated carbon using the Langmuir and Freundlich isotherm expressions. Separation Science and Technology; 28: 2179-2195.
36. Artkla S, Choi W, Wittayakun J. (2009). Enhancement of catalytic performance of MCM-41 synthesized with rice husk silica by addition of titanium dioxide for photodegradation of alachlor. Environment Asia; 2(1): 41-48.
37. Sharififard H, Soleimani M, Aprea P, Pepe F. (2016). Iron-activated carbon nanocomposite: Synthesis, characterization and application for lead removal from aqueous solution. Royal Society of Chemistry Advances; 6(49): 42845-42853.